Near-edge absorption fine structure and UV photoemission spectroscopy studies of aligned single-walled carbon nanotubes on Si(100) substrates

L. Fleming[a)]
Department of Physics, North Carolina State University, Raleigh, North Carolina 27695

M. D. Ulrich
Physics Division, Army Research Office, Research Triangle Park, North Carolina 27709

K. Efimenko and J. Genzer
Department of Chemical Engineering, North Carolina State University, Raleigh, North Carolina 27695

A. S. Y. Chan and T. E. Madey
Department of Physics and Astronomy and Laboratory for Surface Modification, Rutgers University, Piscataway, New Jersey 08855

S.-J. Oh
Curriculum in Applied and Materials Sciences, University of North Carolina, Chapel Hill, North Carolina 27599

O. Zhou
Department of Physics and Astronomy, Curriculum in Applied and Materials Sciences, University of North Carolina, Chapel Hill, North Carolina 27599

J. E. Rowe
Department of Chemistry, University of North Carolina, Chapel Hill, North Carolina 27599

(Received 1 April 2004; accepted 6 May 2004; published 18 August 2004)

We report near-edge absorption fine structure (NEXAFS) and UV photoemission spectroscopy (UPS) studies of aligned single-walled carbon nanotube films on Si(100) substrates. Orientation of the films was detected in the NEXAFS spectra, with the intensity of the π^* core exciton at 284.4 eV showing a strong dependence on nanotube alignment with respect to the polarization of the incident radiation. At lower angles of incidence, the intensity of the π^* peak was higher for all orientations, which we attribute to the greater accessibility of the π^* orbitals. UPS spectra of the films showed little angular dependence and included features consistent with the total density of states of graphite. As a result of the nanotube curvature and the distribution of nanotube chiralities, the UPS spectra are similar to angle-integrated graphite spectra. © *2004 American Vacuum Society.*
[DOI: 10.1116/1.1775190]

I. INTRODUCTION

The potential of carbon nanotubes (CNTs) as future nanoscale device candidates has been confirmed by numerous studies of their intrinsic properties. It is well known that CNTs can be either metallic or semiconducting depending on their chirality, giving them a versatility not found in other materials. The main barriers to the use of nanotubes in applications have been control of the properties in synthesis and the separation and patterning of the nanotubes. Progress in the latter has made field emission devices the first commercial technologies to take advantage of their aspect ratio and electronic properties.[1,2] The eventual assembly of more complicated molecular electronic devices, such as interconnects with conventional complementary metal-oxide-semiconductor field-effect transistors, is anticipated.

We have employed ultraviolet photoemission spectroscopy (UPS) and near-edge absorption fine structure (NEXAFS) to characterize electronic properties of aligned CNT films on a Si(100) substrate. Photoemission extracts information about the binding energies of the initial states of the emitted photoelectrons by measuring their kinetic energies. It is commonly used to determine the dispersion of valence band electronic levels E(k) in crystalline materials. NEXAFS probes the empty states above the Fermi level. Because NEXAFS detects transitions in carbon from the highly isotropic 1s core level, any polarization dependence will reflect the anisotropy of the final states. Hence NEXAFS is ideal for studying ordered systems of π electrons. In our samples, single-walled carbon nanotubes (SWNTs) were deposited in an oriented fashion on Si(100) substrates. We focus on explaining the anisotropy of the electronic states of these films, and on understanding the valence band electronic structure of the nanotubes themselves. Previous photoemission and x-ray absorption studies of CNTs have been performed mainly on either aligned or randomly oriented multiwalled nanotubes, or on randomly oriented SWNT films.[3–7] In most of these, the electronic structure of the nanotubes was found to be largely similar to that of graphite. Valence band spectral features common to both graphite and nanotubes are easily identified, but are significantly broader for the nanotube spectra. In x-ray absorption spectra, chemical vapor deposition (CVD)-grown multiwalled nanotubes have broader π^*

a)Electronic mail: lbflemin@unity.ncsu.edu

and σ^* peaks than graphite as a result of defects, while SWNTs show a stronger similarity.[6,7]

There are some difficulties associated with measuring the electronic structure of bulk CNT samples. Multiwalled nanotubes are comprised of concentric shells, with the total density of states (DOS) approximately representing a sum over the DOS of the layers.[8] Single-walled samples represent a range of chiralities with different electronic properties. Defect states, especially in CVD-grown materials, will contribute to the spectra. Additionally, contamination from residual metal catalyst or graphite particles may also interfere. We have tried to minimize some of these difficulties by using ordered, self-assembled films of cut SWNT bundles.

II. EXPERIMENTAL DETAILS

A. Growth of the aligned self-assembly films

The aligned CNT samples used in this study were prepared using a self-assembly technique described elsewhere.[9] Briefly, the SWNTs were first grown by pulsed laser vaporization, purified by reflux in H_2O_2, and cut by sonication in concentrated acid to approximately 1 μm in length. The purified CNTs are grouped in bundles of about 30–50 nm in size as measured by transmission electron microscopy;[10] cut nanotube bundles are of similar diameter or smaller because of the etching procedure. After cutting, the bundles were suspended in water. They do not separate into individual nanotubes. They remain in suspension for days without sonication or other agitation. Si(100) wafers were prepared by etching in HF for 30 s followed by rinsing in deionized water. After being cut into approximately 1 cm$\times$6 cm pieces, the silicon was then UV cleaned and hung vertically in the CNT suspension. As the water evaporated, nanotube bundles deposited as aligned continuous films along the air/water/substrate line of contact. After deposition, the films were heated on a hotplate to 120 °C for 5 min to remove excess moisture. The samples were then transported to the National Synchrotron Light Source (NSLS) for x-ray absorption and photoemission spectroscopy measurements. The film thicknesses of the samples were not directly measured, but are expected to be in the 0.1–1 μm range based on measurements of other samples.[9] While no complementary technique was used to verify the alignment of these samples, the alignment of previously grown films has been demonstrated by polarized microscopy and polarized Raman spectroscopy.[9]

B. NEXAFS measurements

NEXAFS measurements were conducted at the U7A beamline of the NSLS. The U7A beamline has an effective energy range of 180 to 1200 eV with a resolution of about 0.1 eV at the carbon edge. The beam spot size at normal incidence is 0.5$\times$0.5 mm. Electron yield detection is at 45° with respect to the incident beam and polarization vector, and located in the plane of incidence. The detector is a fully shielded channel electron multiplier with a 50 mm cone and a three-grid high-pass electron kinetic energy filter. The detector was operated in a partial electron yield mode, with the high-pass grid at a -150 V retarding potential. NEXAFS spectra were collected with the CNT/Si(100) film oriented with the nanotube axis (**c**) both parallel ($\parallel$) and perpendicular ($\perp$) to the polarization vector and at polar angles of 90° (normal incidence), 50° and 20° with respect to the incident beam. Each orientation and angle is illustrated in Fig. 1.

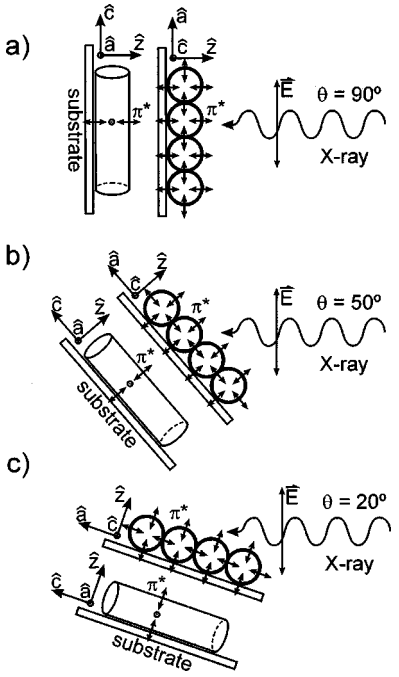

FIG. 1. NEXAFS experimental geometries, showing the two orientations and three angles used. The vector **c** is parallel to the nanotube axis and **z** is perpendicular to the substrate, while **E** is the polarization direction of the incident light. The angles are (a) 90° (b) 50°, and (c) 20°. At 20°, more π^* orbitals (represented by arrows) are aligned with the polarization direction.

C. UPS measurements

UPS spectra were taken at the U4A beamline of the NSLS. The U4A beamline is equipped with a set of spherical grating monochromators that provide a tunable energy range of 10–250 eV and a resolution of 0.1 eV. The beam spot size for normal emission is 0.5$\times$5 mm. Photoelectron kinetic energies were measured using a Vacuum Science Workshop (VSW) hemispherical analyzer at a fixed angle of 45° from the beam direction, and in fixed pass energy mode. The analyzer has an angular resolution of 2°. Before taking data, each sample was annealed at $\sim$500 °C *in situ* under ultrahigh vacuum ($\sim 1\times10^{-10}$ Torr) to remove adsorbates. The spectra were acquired using three different take-off angles: 45° (normal incidence), 90° (normal emission), and 125°. The beam spot size for normal emission is 0.5$\times$5 mm.

III. EXPERIMENTAL RESULTS

A. NEXAFS spectra

NEXAFS spectra of the nanotube films show two prominent peaks, at 284.4 eV and 288.0 eV, corresponding to π^* and σ^* excitons, respectively (Fig. 2). Features above

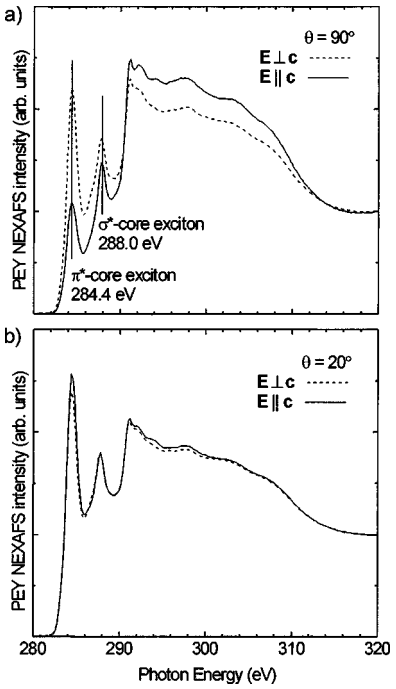

FIG. 2. (a) NEXAFS spectra taken at normal incidence show a large intensity dependence of the π^* core exciton on orientation. (b) The spectra are independent of orientation at low angles of incidence (θ=20°).

290 eV reflect transitions to the continuum states above the Fermi level. All of the spectra were set to zero at 280 eV and normalized to one at 320 eV. The polarization properties indicate significant alignment. In Fig. 2(a), the intensity of the π^* exciton peak is much stronger for the perpendicular orientation than for the parallel orientation at θ=90° (normal incidence). This effect disappears at glancing angles, as can be seen in Fig. 2(b) for the data taken at θ=20°. Figure 3 illustrates the increase in intensity of the π^* exciton peak as the angle of incidence is reduced, while maintaining the nanotube orientation.

B. UPS results

Shown in Fig. 4 are valence band photoemission spectra of the aligned CNT film on Si(100), taken at four photon

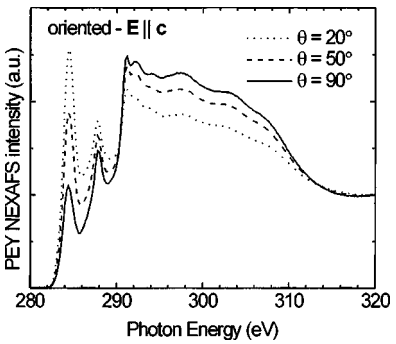

FIG. 3. NEXAFS spectra showing the intensity dependence of the exciton peaks on angle of incidence (shown for **E**∥**c**). The π^* dependence is very strong.

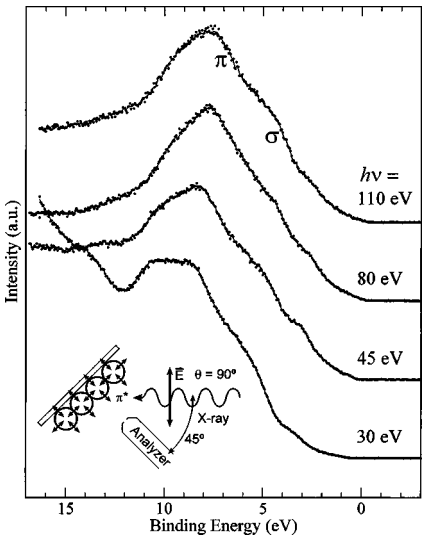

FIG. 4. UPS spectra of the aligned CNT films at θ=90° and four photon energies. σ and π features appear at energies similar to those in graphite, while the overall spectral shape is consistent with an angle-integrated graphite spectrum.

energies. The data shown are for the perpendicular orientation only, at a 90° take-off angle (see Fig. 4 inset). The observed features are broad and overlapping, with some features distinguishable only as shoulders in the overall valence band. π and σ components are marked on the 110 eV spectrum. The CNT UPS data are relatively insensitive to changes in the photon energy or the take-off angle. In Fig. 4, the spectra are all very similar in shape, except for the 30 eV spectrum. Here, the data appear flatter over the 7–10 eV binding energy region, with a prominent secondary electron contribution at higher binding energies. It was also noticed

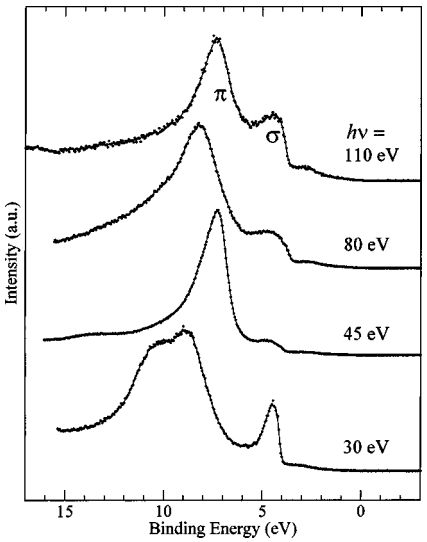

FIG. 5. UPS spectra of graphite using θ=90° and the same set of photon energies as for the CNT spectra. The π band feature shifts with photon energy, while the σ band position is largely independent. This behavior is adequately interpreted using the dispersion relations along the $\Gamma-A$ portion of the Brillouin zone.

that the σ contribution appears stronger for the perpendicular orientation at lower photon energies. Finally, at 30 eV, the π bands have higher intensities with larger take-off angles. For comparison, Fig. 5 shows UPS spectra of graphite at identical photon energies. In contrast to the CNT spectra, the data exhibit sharp peaks and show a dependence on photon energy.

IV. DISCUSSION

A. NEXAFS

The π^* exciton shows a clear dependence on orientation at 90°, as shown in Fig. 2(a), and also at 50° (not shown), indicating good alignment of the films. However, at 20° this effect disappears. The independence of the NEXAFS spectra on orientation at low angles of incidence can be explained by examining the experimental geometries in Fig. 2. Electron excitation is expected to go as $\mathbf{E}\cdot\mathbf{n}$, where $\mathbf{E}$ is the electric field vector and $\mathbf{n}$ is directed along the orbital. For π^* orbitals, $\mathbf{n}$ is directed normal to the surface of the nanotube. At $\theta=90°$ [Fig. 2(a)], π^* orbitals along the sides of the tubes will be accessible to the field when the nanotubes are oriented perpendicular to the polarization. For the parallel orientation, $\mathbf{E}\cdot\mathbf{n}\sim 0$ and hence no excitation is expected. The samples are not perfectly aligned, so that a peak is still observed, but at reduced intensity. At $\theta=20°$, the component of the π^* orbitals normal to the substrate is always accessible, regardless of the orientation.

It is noted here that the normalizations of the NEXAFS spectra did not lead to identical intensities in the continuum region for each orientation, as can be seen in Fig. 2(a). The reason for this is not clear. While it is possible that this difference has affected the measured peak intensities, the difference among the spectra is expected to be less near 280 eV than in the continuum region. Additionally, normalization to the continuum edge instead of to 320 eV would further enhance the differences in the measured peak intensities. In Fig. 2(a), the intensity for the parallel orientation is highest in the continuum region, while its exciton peaks are actually of lower intensity compared to the perpendicular orientation. Because the peaks exhibit the expected intensity behavior with both incidence angle and orientation, we believe that the error due to the background is relatively small. Unfortunately, without identical normalizations it is impossible to obtain quantitative results by fitting the difference spectra in the manner described by Outka *et al.*[11]

A similar trend also appears in the isotropic σ^* exciton. The effect is greatly reduced from the anisotropy detected for the π^* exciton. Though this may partially be explained as a result of the π^* exciton peak overlapping the σ^* exciton peak, a more complete explanation has not been found. Additionally, some asymmetry can be seen in the σ^* exciton peak, on the low energy side, and may correspond to the lower energy fine structure seen in the $1s\rightarrow\sigma^*$ peak of graphite and SWNT x-ray absorption spectra.[6,7]

B. UPS

A comparison to the valence band photoemission spectra of graphite (Fig. 5) using the same photon energies and scattering geometry is helpful in understanding the nanotube spectra (Fig. 4). Graphite spectra exhibit very sharp π and σ band features compared to CNTs. Because of the normal take-off geometry, the $k_{\|}$ component of the photoelectron wave vector is exactly zero and the measurements probe the $\Gamma-A$ portion of the three-dimensional (3D) graphite Brillouin zone.[12] In the spectra of Fig. 5, there is clear evidence of dispersion in the π band, with the peak shifting in energy from 7 to about 9 eV. The σ band over this region is constant, with a binding energy of 4.0 eV. This agrees very well with the dispersion as calculated in the *ab initio* band structure of Tatar and Rabii (full crystal potential) over the $\Gamma-A$ segment of the Brillouin zone.[13]

The SWNT film has a very different 3D structure from graphite, consisting essentially of rolled up sheets of graphene in close-packed bundles. Even so, the valence electron binding energies correspond well to the energies of the π and σ bands near the Γ point of the graphite Brillouin zone. The broad valence band features and relative insensitivity of the CNT data to photon energy or photoemission geometry indicate that the nanotube spectra can be understood as angle-integrated spectra of graphene. Because the nanotube is a nanometer-scale rolled graphene sheet, photoelectrons ejected both normal and tangential to the nanotube/graphene surface are simultaneously detected. This effect is also observed in the spectra of multiwalled carbon nanotubes.[7] Several other factors also contribute to broadening the nanotube spectra. First, the nanotubes in the samples possess a random chirality distribution over the range of available diameters.[14] Although each nanotube DOS will have van Hove singularities, the nonuniformity results in a random distribution of those singularities. Second, tube–tube interactions are known to broaden the DOS compared to individual nanotubes.[15] In all, the total DOS of bundles of random chirality nanotubes should roughly follow the total DOS for graphene.

V. CONCLUSIONS

Self-assembled films of single-walled carbon nanotubes were studied using NEXAFS and photoemission spectroscopy. The CNT films showed the expected NEXAFS intensity dependence with both the angle of incidence and the orientation of the films. The UPS data are interpreted as angle-integrated spectra of graphite, with the valence band spectra reflecting a total DOS. An angle-resolved study of CNTs using the current techniques is not possible. Although our ultimate goal is to understand and characterize the CNT/Si(100) interface, and present film assembly technique results in films too thick to probe the interface. Additional barriers to measuring the interfacial properties are the tendency of nanotubes to bundle and the difficulty of forming a continuous film of nonbundled SWNTs.

[1]C. Bower, W. Zhu, S. Jin, and O. Zhou, Appl. Phys. Lett. **77**, 830 (2000).
[2]S. J. Oh, Y. Cheng, J. Zhang, H. Shimoda, and O. Zhou, Appl. Phys. Lett. **82**, 2521 (2003).
[3]S. Suzuki, C. Bower, T. Kiyokura, K. G. Nath, Y. Watanabe, and O. Zhou, J. Electron Spectrosc. Relat. Phenom. **114–116**, 225 (2001).
[4]S. Suzuki, Y. Watanabe, T. Kiyokura, K. G. Nath, T. Ogino, S. Heun, W. Zhu, C. Bower, and O. Zhou, Phys. Rev. B **63**, 245418 (2001).
[5]K. Umishita, Y. Ochiai, K. Iwasaki, and S. Hino, Synth. Met. **121**, 1159 (2001).
[6]R. Larciprete, S. Lizzit, S. Botti, C. Cepek, and A. Goldoni, Phys. Rev. B **66**, 121402(R) (2002).
[7]J. Schiessling, L. Kjeldgaard, F. Rohmund, L. K. L. Falk, E. E. B. Campbell, J. Nordgren, and P. A. Brühwiler, J. Phys.: Condens. Matter **15**, 6563 (2003).
[8]L. Forró and C. Schönenberger, in *Carbon Nanotubes: Synthesis Structure, Properties, and Applications*, edited by M. S. Dresselhaus, G. Dresselhaus, and P. Avouris (Springer, Berlin, 2001), pp. 205–272.
[9]H. Shimoda, S. J. Oh, H. Z. Geng, R. J. Walker, X. B. Zhang, L. E. McNeil, and O. Zhou, Adv. Mater. (Weinheim, Ger.) **14**, 899 (2002).
[10]H. Shimoda, B. Gao, X.-P. Tang, A. Kleinhammes, L. Fleming, Y. Wu, and O. Zhou, Phys. Rev. Lett. **88**, 015502 (2002).
[11]D. A. Outka, J. Stöhr, J. P. Rabe, and J. D. Swalen, J. Chem. Phys. **88**, 4076 (1987).
[12]D. Marchand, C. Frétigny, M. Laguës, F. Batallan, Ch. Simon, I. Rosenman, and R. Pinchaux, Phys. Rev. B **30**, 4788 (1984).
[13]R. C. Tatar and S. Rabii, Phys. Rev. B **25**, 4126 (1982).
[14]X.-P. Tang, A. Kleinhammes, H. Shimoda, L. Fleming, K. Y. Bennoune, S. Sinha, C. Bower, O. Zhou, and Y. Wu, Science **288**, 492 (2000).
[15]J. P. Lu and J. Han, Int. J. High Speed Electron. Syst. **9**, 101 (1998).